Hybrid Compound Design To Overcome the Gatekeeper T338M Mutation in cSrc[#]

Matthäus Getlik,[†] Christian Grütter,[†] Jeffrey R. Simard, Sabine Klüter, Matthias Rabiller, Haridas B. Rode, Armin Robubi, and Daniel Rauh*

Chemical Genomics Centre of the Max Planck Society, Otto-Hahn-Strasse 15, D-44227 Dortmund, Germany

The emergence of drug resistance remains a fundamental challenge in the development of kinase inhibitors that are effective over long-term treatments. Allosteric inhibitors that bind to sites lying outside the highly conserved ATP pocket are thought to be more selective than ATP-competitive inhibitors and may circumvent some mechanisms of drug resistance. Crystal structures of type I and allosteric type III inhibitors in complex with the tyrosine kinase cSrc allowed us to employ principles of structure-based design to develop these scaffolds into potent type II kinase inhibitors. One of these compounds, **3c** (RL46), disrupts FAK-mediated focal adhesions in cancer cells via direct inhibition of cSrc. Details gleaned from crystal structures revealed a key feature of a subset of these compounds, a surprising flexibility in the vicinity of the gatekeeper residue that allows these compounds to overcome a dasatinib-resistant gatekeeper mutation emerging in cSrc.

Introduction

Kinases and their associated signaling pathways are responsible for the regulation of intracellular processes. Aberrant kinase regulation can have a significant effect on the dynamics of these intricate networks, ultimately resulting in total cellular disregulation and contributing to the onset of several diseases including cancer.[1] On the basis of an improved understanding of kinase malfunction in cancer biology, small organic molecules have been developed for targeted cancer therapy. Although a dozen kinase inhibitors are on the market and several more are in clinical trials, inhibitor selectivity, lack of efficacy, and the emergence of drug resistance remain fundamental challenges in the development of kinase inhibitors that are effective in long-term treatments.[2−5] This can be attributed to the fact that most kinase inhibitors are ATP-competitive molecules (type I inhibitors), such as staurosporine and the dual specific Src/Abl[a] inhibitor dasatinib, which bind in the highly conserved ATP pocket and form a critical hydrogen bond with the hinge region of the kinase domain. Therefore, allosteric inhibitors that bind to less conserved sites outside the ATP pocket would be expected to have improved selectivity profiles and offer new opportunities for scaffold development.[6]

We sought to use structure-based design principles to develop organic molecules that stabilize an enzymatically inactive conformation of the cSrc kinase domain while maintaining potency against a particular mutation (T338M) at the gatekeeper residue, an amino acid situated at the back of the ATP pocket that is well-known for influencing type I inhibitor affinity and selectivity profiles among kinases,[7] of cSrc which results in
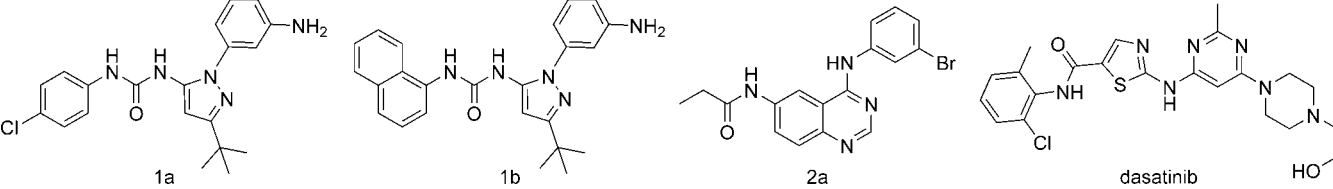
resistance to dasatinib. cSrc is known to be overexpressed or up-regulated in several tumor types, most notably in glioblastoma, gastrointestinal, and prostate cancers, and represents a target kinase for tumor therapy.[8−11] In addition, our investigation was stimulated by (a) type II kinase inhibitors such as lapatinib and imatinib which not only bind in the ATP pocket but also extend past the gatekeeper residue into a less conserved adjacent allosteric site that is present solely in inactive kinase conformations and (b) a series of recently discovered type III inhibitors that bind exclusively in the allosteric site of inactive cSrc without making contact with the hinge region or the gatekeeper. Type II inhibitors essentially stabilize this inactive conformation and very often have slow dissociation rates, resulting in significantly increased affinities over type I inhibitors.[6] However, resistance mutations are emerging at an increasingly rapid pace and often limit the success of type I and type II inhibitors employed in new targeted cancer therapies. The most common mutations occur at the gatekeeper position in the hinge region[12] in which a small amino acid side chain (classically Thr) is exchanged for a larger hydrophobic residue (Ile or Met). Such mutations have been thoroughly investigated (breakpoint cluster region−Abelson kinase (Bcr-Abl) (T315I), mast-stem cell growth factor receptor kinase (c-KIT) (T670I), platelet derived growth factor receptor (PDGFRα) (T674I), and epidermal growth factor receptor (EGFR) (T790M); cSrc (T338M) was previously used as a model system relevant to other drug resistant kinases[13,14]) and shown to cause a steric clash that impedes the binding of ATP-competitive inhibitors, increase enzymatic activity, or increase the affinity for ATP of some kinases.[15−17] Given the high mutation rate of tumor cells, the treatment of patients with reversible inhibitors likely selects for pre-existing cancer cell lines expressing the drug-resistant kinases. However, the example of the Aurora kinase inhibitor VX-680, which retains weak activity against drug-resistant T315I Bcr-Abl kinase mutant[18,19] (PDB code 2F4J) by extending out and away from the hinge region and circumventing the gatekeeper residue, shows that in principle reversible inhibitors can be obtained that overcome drug resistance. It would therefore be desirable to identify new chemical principles that can bind "around" these mutations or target the kinase outside the ATP pocket and lock it in an enzymatically inactive conformation.

Table 1. Type I and Type III Inhibitors of cSrc and p38α[a]

compd	IC$_{50}$ (μM)		K$_D$ (μM)	
	cSrc (wild type)	cSrc (T338M)	cSrc (wild type)	p38α
1a	32.1 ± 7.5[20]	27.8 ± 10.2	35 ± 0.9%[20] at 50 μM	0.055[20] ± 0.005
1b	64.1 ± 15.3[20]	nb	26 ± 1.3%[20] at 50 μM	0.012[20] ± 0.002
2a	6.4[14]	nb[14]	45 ± 1.3%[20] at 10 μM	nm*
dasatinib	0.0004 ± 0.0002	0.480 ± 0.40	0.011 ± 0.003	0.495 ± 0.128*

[a] Structures of pyrazoloureas **1a**, **1b**, and 4-aminoquinazoline **2a** are shown. IC$_{50}$ values for inhibited enzyme activity (in μM) for a panel of inhibitors against wild type (no drug resistance mutation at the gatekeeper) and drug resistant cSrc (cSrc-T338M). K$_d$ values (in μM) for the same panel of pyrazoloureas in cSrc and p38α. Pyrazoloureas **1a**, **1b** are potent inhibitors of p38α. Inhibitor **1a** demonstrates balanced inhibition of wild type and drug resistant cSrc-T338M, while bulky naphthyl derivative **1b** weakly inhibits cSrc but fails to inhibit cSrc-T338M most likely because of a steric clash with the larger gatekeeper residue (Supporting Information Figure 2). Quinazoline **2a** was weakly sensed by acrylodan-labeled p38α but was strongly detected by acrylodan-labeled cSrc as a weak type I inhibitor that binds to the hinge region of the kinase. The large bromophenyl moiety clashes with the gatekeeper side chain in drug resistant cSrc-T338M and results in significant drop in affinity.[14] The asterisk "*" denotes compounds for which K$_d$ values were not measureable (nm) because of high interference by intrinsic compound fluorescence. Acrylodan-labeled p38α exhibits an insensitivity to type I binders, unlike fluorescent cSrc, while both fluorescent kinases serve as excellent sensors for DFG-out binders.

The above-mentioned allosteric site is formed when the activation loop, a crucial structural component of the substrate binding cleft participating in the recognition of substrates and influencing the arrangement of the catalytic residues, adopts the DFG-out conformation that is characteristic of inactive kinases. In this conformation, the Phe of the DFG motif partially blocks the ATP binding site, leaving the allosteric site available for ligand binding. The equilibrium between the active DFG-in and inactive DFG-out conformation can be modulated by phosphorylation of the activation loop, by a variety of protein−protein interactions, or by the binding of type I, II, or III inhibitors to particular protein conformations.

The recent availability of structural information of inactive kinase conformations (p38α, EGFR, Abelson kinase (Abl), vascular endothelial growth factor receptor (VEGFR), and B-RAF) in complex with type II or type III inhibitors has intensified the search for novel inhibitor scaffolds and stimulated us to develop a direct binding assay that allowed for the first time the unambiguous identification and discrimination of organic molecules that target kinases of interest outside the ATP pocket and stabilize the kinase domain in an enzymatically inactive conformation.[20] This new assay system reports on structural changes of the activation loop associated with ligand binding and enabled us to discover a series of pyrazoloureas as truly allosteric binders (type III inhibitors) to the tyrosine kinase cSrc. We employed protein X-ray crystallography to confirm that these compounds bind to the DFG-out conformation and lock the kinase in its inactive state. Here, we investigate the pharmacological relevance of targeting this site in cSrc by using principles of fragment-based drug design to systematically develop a series of type II inhibitors that potently inhibit cSrc in the low nanomolar range. We further demonstrate through kinetic and structural analysis that a subset of these inhibitors (**3a**−**c**) has surprising structural plasticity and is capable of overcoming the emerging mechanism of gatekeeper-associated drug resistance in kinases. We also demonstrated that one such molecule, **3c**, blocks proliferation of cancer cells by directly inhibiting the tyrosine kinase cSrc and disrupting the formation of cellular focal adhesions mediated by a substrate of cSrc, focal adhesion kinase (FAK).

Results

Type III Inhibitors Active on Drug Resistant cSrc. We recently developed a novel assay system that detects the binding of type II and type III allosteric kinase modulators of the tyrosine kinase cSrc by directly sensing the conformational changes that they induce in the activation loop of the kinase. To achieve this, we introduced the point mutation L407C into the activation loop of the kinase to allow subsequent labeling with acrylodan, a fluorophore sensitive to polarity changes of its environment.[20] Conformational changes associated with the binding of allosteric inhibitors bring the fluorophore toward the cleft between the C and N lobes of the kinase, thereby modifying its fluorescence characteristics. In a screening campaign, we employed this newly developed cSrc assay to identify pyrazolourea compounds (**1a,b**) as type III allosteric binders to cSrc with K$_d$ values in the micromolar range (Table 1). Although the binding of type III inhibitors had not been reported previously for cSrc kinase, several pyrazoloureas are known to be potent type III binders of the serine/threonine kinase p38α MAP kinase with affinities in the low nanomolar range.[21,22] Enzyme activity assays were subsequently used to confirm inhibition of cSrc kinase activity in the micromolar range (Table 1), and the proposed type III allosteric binding mode was confirmed by protein X-ray crystallography (PDB codes 3F3U and 3F3T). Additionally, these complex structures shed some light on the preference of cSrc for the shared R$_2$ N′-aryl moiety in **1a,b** and highlight that the size and degree of hydrophobicity of these aryl substituents are important determinants for more energetically favorable binding to inactive cSrc kinase conformations. We carried out the same activity assay using the drug resistant cSrc variant (T338M)[13,14] and found that the presence of a bulkier gatekeeper residue had no effect on **1a** potency when compared to wild type cSrc while **1b** appeared to no longer be active against cSrc. This further highlighting the importance of the urea-anilino moiety of **1a** in contributing to its affinity to cSrc, unlike type I inhibitors such as quinazoline **2a** and the aminothiazole dasatinib, which show a dramatic loss in potency in cSrc-T338M (Table 1). Similar observations have also been reported for
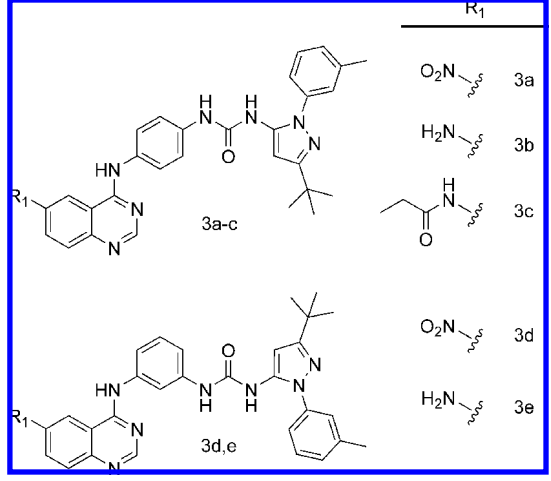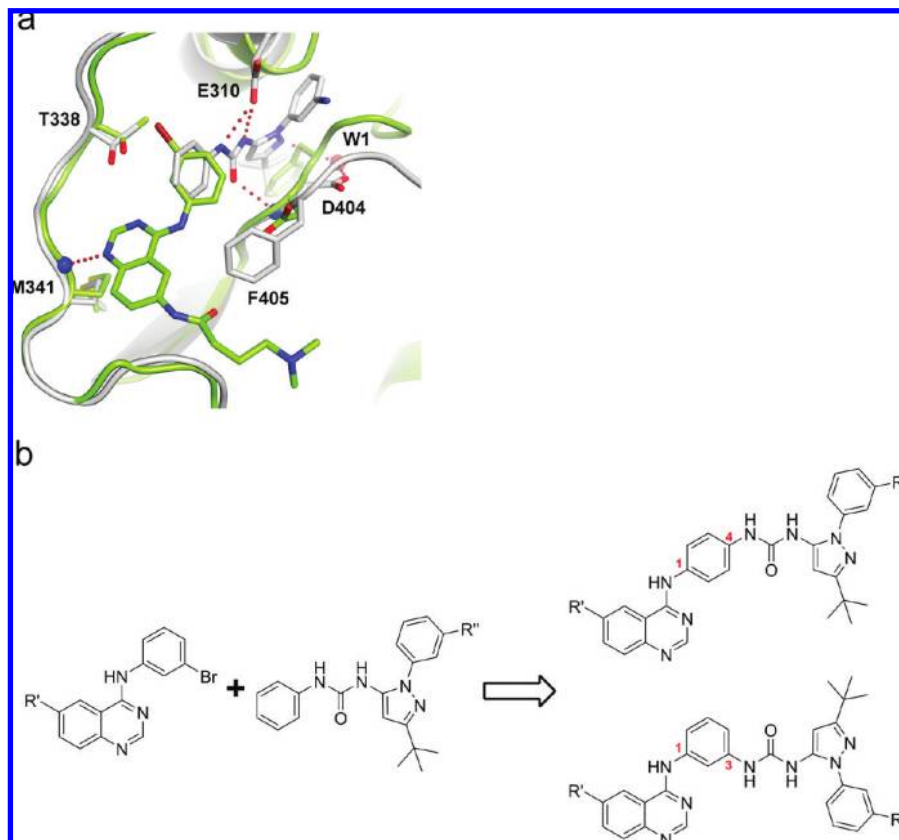
Figure 1. Structure-based design of potent type II hybrid inhibitors of cSrc kinase. (a) The cocrystal structures of cSrc in complex with a pyrazolourea type III inhibitor (PDB entry 3F3U)[20] (gray) aligned with the structure of cSrc in complex with an ATP-competitive 4-aminoquinazoline (green) (PDB entry 2QLQ)[14] provided the rationale for structure-based drug design. The quinazoline core binds to the hinge region of the kinase, while the pyrazolourea exclusively binds to the allosteric site of the kinase. The planes of the phenyl moieties of both inhibitors align adjacent to the Thr338 gatekeeper residue in chicken cSrc. (b) Rationally designed type II inhibitors based on the binding modes of type I 4-aminoquinazolines and type III pyrazoloureas bound to cSrc. According to the notion of fragment-based drug discovery,[25,26] chemically combining the two weak binders should result in significantly higher binding affinities.

EGFR, where the T790M gatekeeper mutation results in resistance to the marked drugs gefitinib and erlotinib.[23] To better understand the mechanism of dasatinib resistance in cSrc, we solved its crystal structure in complex with wild type cSrc and modeled the found binding mode to apo cSrc-T338M (PDB code 2QI8) (see Supporting Information Figure 1 and Supporting Information methods). The alignment clearly shows that the larger Met side chain of the mutant variant not only eliminates an essential hydrogen bond of the inhibitor to the gatekeeper side chain (T338) but also sterically impedes inhibitor binding. The same steric repulsion by the larger gatekeeper residue is likely responsible for the loss of activity of **1b** and **2a** in cSrc-T338M (see Supporting Information Figure 2) and highlight that a larger gatekeeper residue is not expected to interfere with compounds that have the optimal size and degree of hydrophobicity to bind behind the gatekeeper position and exclusively within the allosteric pocket of inactive kinase conformations (DFG-out) such as **1a**.

Design of Potent Type II Hybrid Inhibitors for cSrc Kinase. Given the moderate micromolar IC$_{50}$ values of the type III pyrazoloureas **1a,b** in cSrc, we set out to design more potent type II cSrc inhibitors. We superimposed one of our cSrc-pyrazolourea complexes (PDB code 3F3U) with one of our recently solved cSrc structures in complex with a 4-amino-quinazoline[14] (PDB code 2QLQ) and found that the phenyl substituents of both inhibitor scaffolds (aniline of the quinazoline and aniline of the pyrazolourea) nicely align near the Thr338 gatekeeper side chain (Figure 1a), suggesting that a more potent

inhibitor could be generated by fusing both scaffolds via a 1,4- or 1,3-substituted linkage (Figure 1b). Similar pyrazoloureas fused to various hinge region binders are claimed in patent literature to inhibit TIE-2 and RAF-kinase activity.[24] In our investigations, we were stimulated by both fragment-based design approaches (where molecule fragments identified by NMR[25] or protein X-ray crystallography[26,27] can be efficiently linked or grown to generate molecules with increased affinity) and the emerging concepts of the rational design of DFG-out binders.[6,28] Both methods have been proven to be powerful in kinase lead discovery projects.[29,30] Since pyrazoloureas have been shown to be privileged motifs for the allosteric inhibition of p38α and bind behind the mutation-prone gatekeeper residue, we wanted to employ these scaffolds as starting points for structure-guided design processes that take into account larger gatekeeper side chains. We docked the proposed 1,4-para and 1,3-meta hybrid compounds into a published structure of BIRB-796 bound to the DFG-out conformation of p38α[22] and observed different binding site geometries in the vicinity of the gatekeeper residue and the hinge region in p38α when compared to inactive cSrc (see Supporting Information Figure 3). Given these observations, we predicted that cSrc would better accommodate hybrid compounds fused via a 1,4-para linkage while a 1,3-meta linkage should favor binding to p38α. More importantly, we predicted that the 1,4-substitution pattern in these compounds would provide the optimal geometry to avoid steric clashes with the larger amino acid side chains found at the gatekeeper position of drug resistant kinases. Although the 4-amino-

Table 2. Focused Library of Rationally Designed Type II Inhibitors[a]

	IC$_{50}$ (μM)		K_d (μM)	
compd	cSrc (wild type)	cSrc (T338M)	cSrc (wild type)	p38α
3a	0.071 ± 0.010	0.101 ± 0.004	0.174 ± 0.038	0.127 ± 0.026
3b	0.021 ± 0.005	0.034 ± 0.012	0.073 ± 0.016	0.342 ± 0.039
3c	0.014 ± 0.001	0.023 ± 0.004	0.056 ± 0.013	0.245 ± 0.055
3d	0.207 ± 0.079	nb	0.256 ± 0.064	0.050 ± 0.016
3e	0.235 ± 0.094	36.8 ± 6	0.239 ± 0.045	0.074 ± 0.002

[a] Structures of 1,4-para (**3a**−**c**) and 1,3-meta (**3d,e**) quinazoline−pyrazolourea hybrid compounds are shown. IC$_{50}$ and K_d values (in μM) for a panel of inhibitors against wild type cSrc, drug resistant cSrc-T338M, and p38α. 1,4-Substituted hybrids show the best balance of potency and selectivity for cSrc (wild type and drug resistant). The R$_1$ substituents in position 6 of the quinazoline core are important determinants for potency in cSrc and render a clear SAR with **3c** being the most potent hybrid compound for both cSrc wild type and drug resistant cSrc-T338M. 1,3-Substituted inhibitor cores direct selectivity of (**3d,e**) toward p38α and significantly decreases affinity to drug resistant cSrc-T338M.

quinazoline **2a** and the identified pyrazoloureas **1a** and **1b** are alone weak inhibitor fragments with IC$_{50}$ values in the micromolar range in wild type cSrc, we expected that the resulting 1,4-substituted hybrid compounds would show significantly increased potency in inhibiting not only wild type but also the otherwise drug resistant cSrc-T338M mutant variant.

Synthesis of a Focused Library of 4-Aminopyrazoloureaquinazolines as Novel Type II Inhibitors. We synthesized a small focused library of fused quinazoline−pyrazolourea hybrids as potent type II inhibitors of cSrc (Table 2 and Scheme 1). The panel included analogues with varying inhibitor geometries designed to orient around the sterically bulky gatekeeper residue of drug resistant cSrc-T338M or to preferentially bind to p38α, a kinase that is known to be inhibited potently by compounds containing the pyrazolourea scaffold. Detailed synthetic procedures are described in the Experimental Section.

In Vitro Characterization of Novel Type II Hybrid cSrc Inhibitors. To test whether the allosteric site in cSrc confirmed by our previous cocrystallization experiments is indeed druggable in solution and to test the above-mentioned hypotheses regarding inhibitor selectivity to p38α and drug resistant cSrc-T338M, we first measured the K_d of each hybrid compound using the fluorescent-labeled kinase binding assay described elsewhere.[20] The binding data obtained from each fluorescent kinase confirmed the expected binding preference of 1,4- and 1,3-substituted hybrid compounds for cSrc and p38α, respectively. Additionally, we performed enzyme activity assays for cSrc (wild type and drug resistant T338M) using several type II hybrid compounds (Table 2) to confirm inhibition of

phosphotransfer. We observed a significant (up to 4 orders of magnitude) increase in potency in the measured IC$_{50}$ values of these compounds when compared to the pyrazolourea (**1a**, **1b**) or quinazoline (**2a**) moieties that were used to construct each type II hybrid. The absolute values of the measured K_d values are slightly higher when compared to the IC$_{50}$ values but follow the same trends for 1,4- and 1,3-substituted hybrid compounds. Last and most important, the kinetics clearly demonstrate that the 1,4-substituted hybrid compounds (**3a**−**c**) show no loss of potency in the drug resistant cSrc-T338M mutant in vitro.

Complex Crystal Structures of Novel Type II Inhibitors in cSrc and Drug Resistant cSrc-T338M Mutant Variant. To get deeper insights into the binding mode of this class of type II inhibitors and to understand how these 1,4-substituted inhibitors can overcome a bulky Met gatekeeper residue to inhibit kinase activity without penalty of their affinity, we cocrystallized cSrc (wild type and drug resistant T338M) with RL45 (**3b**) and found that the compound indeed binds to the DFG-out conformation and adopts the proposed type II inhibitor binding mode that spans from the allosteric site into the distal ATP binding pocket (Figure 2). The N1 of the quinazoline moiety makes direct hydrogen bonding interactions with the hinge region (M341) of the kinase, which is typically observed for quinazoline binding to cSrc,[14] cyclin-dependent kinase 2 (CDK2),[31] p38α,[31] Aurora,[32] and EGFR.[33,34] The pyrazolourea moiety resides in the allosteric site and forms identical hydrogen bonding interactions with helix C and the N-terminal region of the activation loop (DFG-motif) as seen for the cSrc−type III inhibitor complexes (PDB codes 3F3U and 3F3T)[20] and as observed in the structure of BIRB-796 complexed to p38α.[22] The central phenyl ring of **3b** that bridges the quinazoline and pyrazolourea scaffolds is sandwiched between the gatekeeper residue and the side chain of F405 of the DFG motif. Interestingly, in the cSrc-T338M-**3b** complex the presence of the sterically demanding Met gatekeeper forces the central phenyl moiety of the inhibitor to rotate 90° to avoid the steric clash with the amino acid side chain such that the plane of the phenyl ring of the inhibitor now faces C$^\varepsilon$ of M338. The side chain of F405 also rotates by 90° to conserve the electrostatically favorable edge-to-face orientation[35] of both π-electron systems (inhibitor phenyl and phenyl side chain of F405) (Figure 2c and Figure 2d), suggesting an additional stabilizing role for this interaction. Rotation of the central phenyl element in 1,3-substituted hybrid compounds **3d** and **3e** is not possible without disrupting the binding orientation of either the quinazoline or pyrazolourea moiety with the protein and provides the explanation for why 1,3-disubstituted hybrids such as **3d** and **3e** do not bind to drug resistant cSrc-T338M (Figure 3). In a recent study, Shokat and colleagues report on a similar flexibility of a pyrazolopyrimidine based type I inhibitor to be able to accommodate either wild type cSrc or a phosphoinositide 3-kinase (PI3K) (Ile at the gatekeeper) to make a dual specific tyrosine kinase (TK)/PI3K inhibitor.[7]

Type II cSrc Inhibitors Disrupt Cell-to-Cell Contacts in cSrc-Dependent Cancer Cell Lines. To assess cSrc inhibition by the most potent 1,4-substituted hybrid **3c** in cellular systems, we treated PC3 and DU145 prostate carcinoma cell lines[10] with different concentrations of **3c**, 100 nM dasatinib (positive Src inhibition control), or vehicle (DMSO). We monitored the phosphorylation state of Y416 (an autophosphorylation site in the activation loop of cSrc) and Y576/Y577 (two residues in the activation loop of FAK that are phosphorylated by cSrc to fully activate FAK). FAK is a nonreceptor tyrosine kinase that

Scheme 1. Synthesis of Quinazoline Derivatives[a]
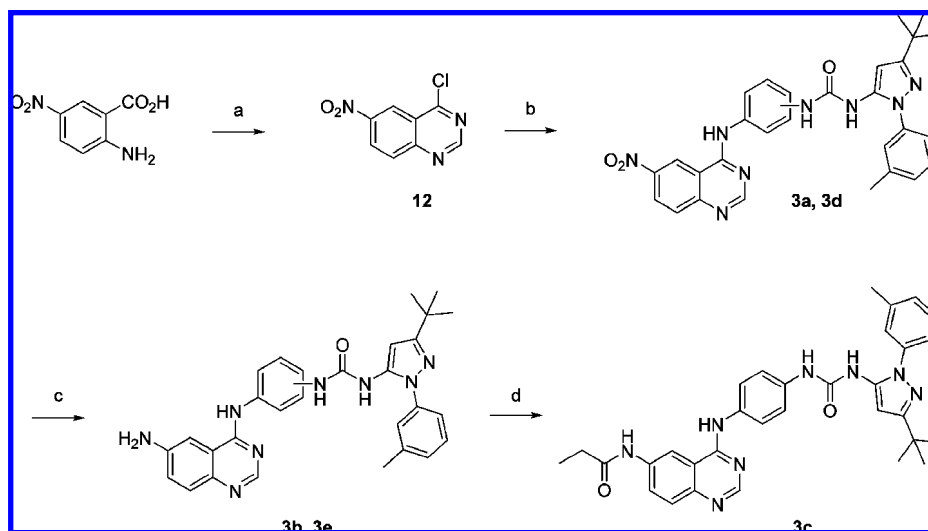
[a] Reagents and conditions: (a) (i) formamidine acetate, 2-methoxyethanol, 132 °C; (ii) SOCl$_2$, cat. DMF, reflux; (b) aminophenylpyrazolourea hydrochlorides, DIPEA, CH$_2$Cl$_2$, room temp; (c) Pd/C, ammonium formate, EtOH, reflux; (d) **3b**, propionyl chloride, DIPEA, THF, 0 °C.

localizes to focal adhesions that form between cells and is a key regulator of cell cycle progression, cell survival, and cell migration.[36] Its activation by cSrc results in the disruption of focal adhesions, causing loss of cell−cell and cell−matrix contacts and apoptosis.[11,37] The overexpression of FAK and cSrc has been shown to lead to increased cell invasion and metastasis in both breast and colon cancers.[38,39]

After 5 h of treatment with dasatinib or **3c**, confluent PC3 and DU145 cells exhibited markedly reduced pSrc (Y416) and pFAK (Y576/Y577) levels (Figure 4a) as well as a loss of cell adhesions and a significant reduction in the number of cells (Figure 4b). Given the reduction of pFAK, this change in cellular morphology is associated with direct inhibition of Src kinase by **3c** via a reduction in downstream signaling through FAK. Interestingly, we also observed an up-regulation of Src expression in both cell lines with increasing **3c** concentration. A positive feedback mechanism involving the up-regulation of Src expression in response to inhibited Src activity has also been observed elsewhere,[40] further suggesting that **3c** shows selectivity toward Src kinase in vivo. In order to determine kinase selectivity for our newly developed type II hybrid compounds, kinase profiling was performed for **3b** and **3e** against a selected panel of 27 different kinases at a concentration of 5 μM (Ambit Biosciences) (see Supporting Information Figure 4).

The combination of in vitro binding and activity assays demonstrates that the quinazoline−pyrazolourea hybrids presented here are promising kinase inhibitor scaffolds for further medicinal chemistry initiatives. The gatekeeper is a Thr in many tyrosine kinases and also serves as a crucial determinant of type I inhibitor selectivity and affinity. Therefore, the development of these type II hybrid inhibitors combined with the observation of a potential cross-talk between the inhibitor and the side chains of the drug resistant hydrophobic gatekeeper and/or the DFG phenylalanine residue provides an attractive chemical biological strategy for developing potent inhibitors that can selectively target such kinases while also overcoming the increasingly common gatekeeper mutation-associated drug resistance.

Discussion and Conclusion

Inhibitor selectivity and the emergence of drug resistance remain fundamental challenges in the development of kinase

inhibitors that are effective in long-term treatments. Here, we present a series of type III inhibitors active on a dasatinib resistant cSrc-T338M mutant variant. Despite weak binding to cSrc in comparison to p38α, these pyrazoloureas served as an excellent starting point for the development of these more potent cSrc inhibitors. On the basis of the analysis of crystal structures of cSrc in complex with different type III pyrazoloureas or with type I quinazoline-based inhibitors, we designed quinazoline−pyrazolourea type II hybrid inhibitors that proved to be excellent cSrc inhibitors. Several derivatives were synthesized to explore SAR and confirmed our prediction that the geometry of these compounds would (i) govern their preferential binding to either cSrc or p38α and (ii) permit the circumvention of larger gatekeeper residues that are known to commonly cause drug resistance in certain cancer cell lines. We were able to confirm these hypotheses by using direct K_d determination (acrylodan-labeled cSrc and p38α), kinase activity assays, and protein X-ray crystallography. The increased affinity of these type II hybrid compounds was not only due to the added 4-aminoquinazoline moiety to make contact with the hinge region of the kinase but also due to the substitution pattern of the central phenyl moiety that is positioned near the gatekeeper residue. Although both 1,4-para and 1,3-meta hybrid compounds inhibit cSrc in the low nanomolar to mid-nanomolar range, only the central phenyl of the 1,4-substituted hybrid overcame the T338M cSrc drug resistance mutation by having the rotational freedom necessary to avoid a clash with the bulkier gatekeeper side chain without also disturbing the binding interactions formed by the rest of the drug molecule. In a recent study, Shokat and colleagues report on a similar flexibility observed in a pyrazolopyrimidine-based type I inhibitor that is accommodated by either wild type cSrc (gatekeeper Thr) or a PI3-kinase (gatekeeper Ile) to serve as a dual-specificity TK/PI3K inhibitor.[7] In a second paper by the same group, the authors report on the design of a series of pyrazolopyrimidinoureas as potent type II cSrc inhibitors.[41] Complex structures with cSrc revealed a para-substituted phenyl ring of the inhibitors in proximity to the gatekeeper. The authors conclude that the relative orientation of this phenyl ring to the *o*-methylphenylamino moiety of imatinib, which is responsible for drug resistance in Abl-T315I, may suggest that these inhibitors can bind to Abl-T315I. The activity of our type II inhibitors in cSrc-relevant prostate cancer cell lines supports
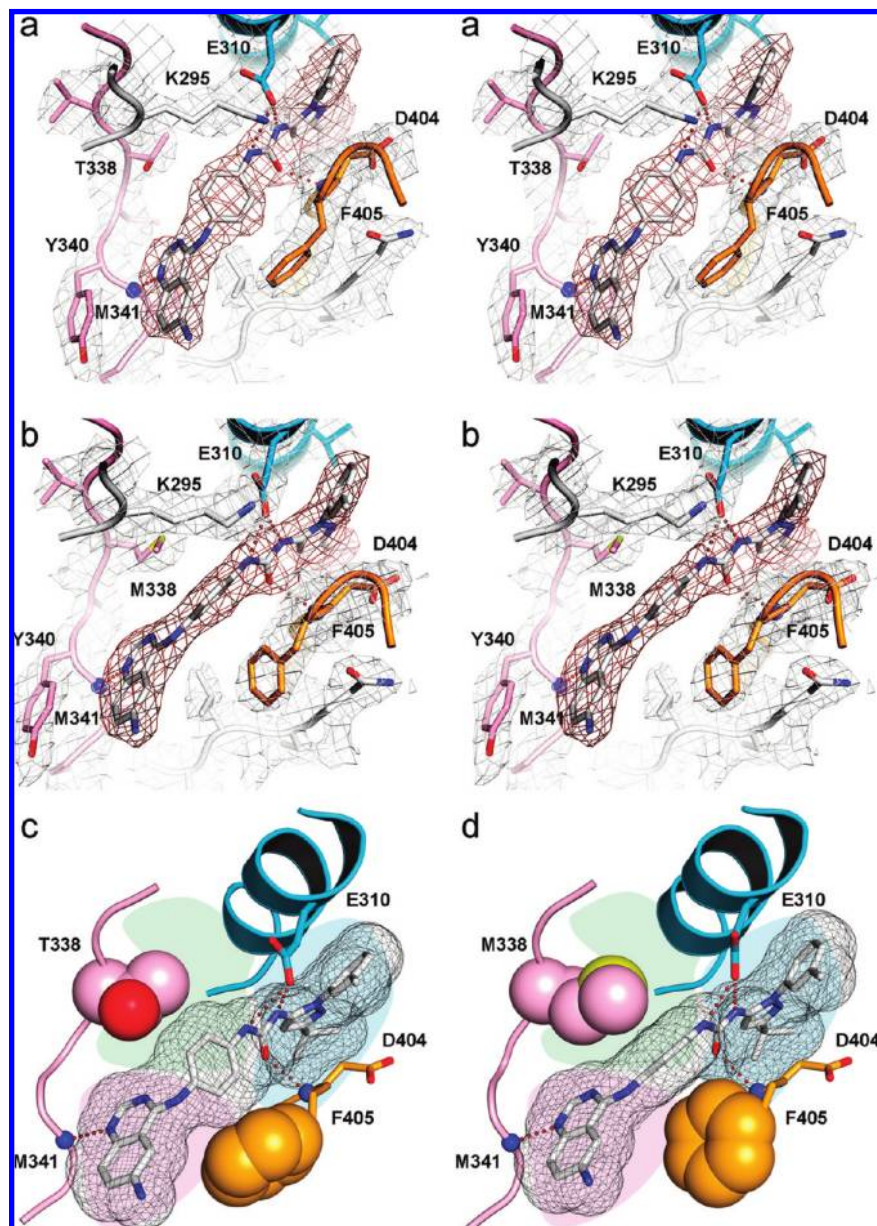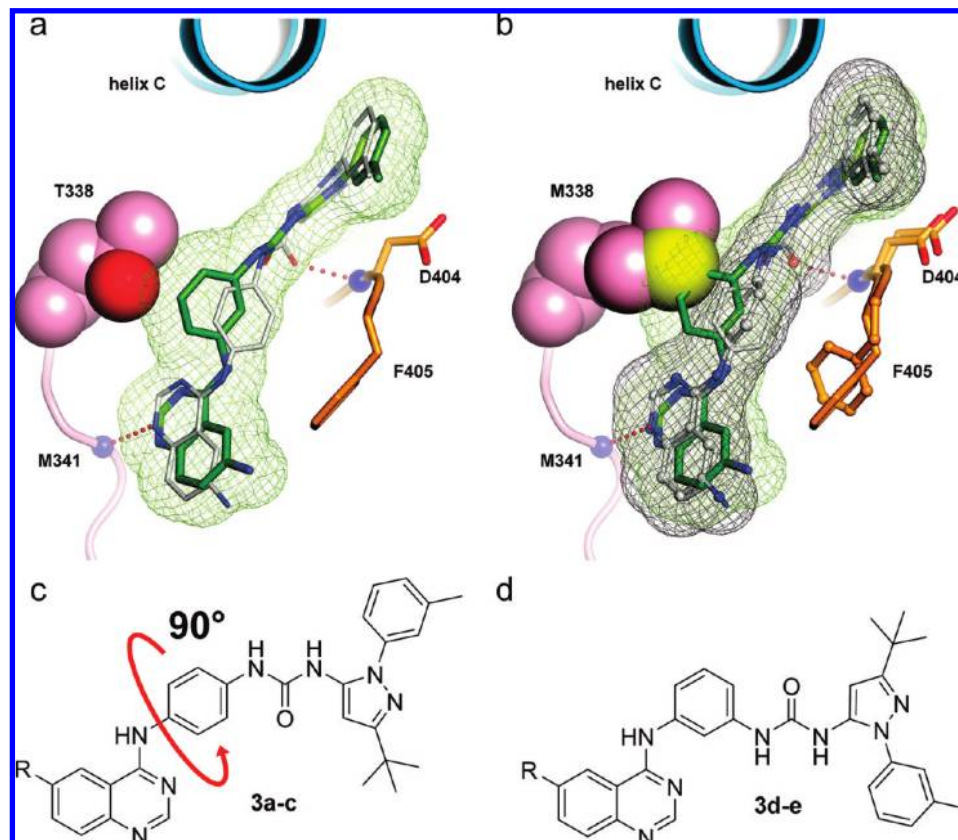
Figure 2. 1,4-Substituted hybrid compound (**3b**) in complex with wild type cSrc and drug resistant cSrc-T338M reveals inhibitor flexibility for overcoming a gatekeeper-associated drug resistance mutation. Stereodiagrams of the experimental electron densities (ligand red, protein gray) of cSrc-**3b** (a) and cSrc-T338M-**3b** (b) both at 2.6 Å resolutions are shown ($2F_o - F_c$ map contoured at 1σ). Hydrogen bonding interactions of the inhibitors with helix C (blue), the DFG-motif (orange), and the hinge region (pink) are shown by red dotted lines. The kinase domain is in the inactive conformation, and the pyrazolourea moiety resides in the allosteric site flanked by helix C and the DFG-motif. N1 of the quinazoline makes a direct hydrogen bond to the main chain amide of M341, which is an interaction commonly formed between anilinoquinazolines and the hinge region of several other protein kinase domains. In both complexes, the central phenyl moiety that links the quinazoline scaffold with the pyrazolourea fragment interacts with the side chain of F405 (DFG motif) in a favorable edge-to-face orientation. (c) van der Waals radii of the inhibitor (mesh), the gatekeeper residues T338/M338 (pink spheres), and the side chain of F403 (orange spheres) explain conformational changes of the central phenyl moiety of the inhibitor to bypass steric clashes with the side chain of M338, allowing **3b** to bind to drug resistant cSrc-T338M. (d) A larger side chain at the gatekeeper position results in a 90° flip of the central phenyl moiety of the inhibitor. Likewise, the side chain of F405 is rotated by 90° to maintain the electrostatically favorable edge-to-face orientation of both π-electron systems conserved.[35]

the structure-based rationale used in the design of these more potent hybrid compounds. It is believed that the in vivo efficacy of drugs against their primary targets is strongly correlated to the drug–target residence time, the concept that a drug remains efficacious only as long as it is bound to its target.[42] In the case of cSrc, we were able to use our acrylodan-labeled cSrc assay to confirm that the 1,4-substituted compounds (**3a**−**c**) dissociate more slowly than the less potent 1,3-substituted compounds (**3d**, **3e**) while the binding rates for all compounds were essentially the same (see Supporting Information Table 2). Although it is not clear which kinases will develop point-

mutation-associated drug resistance under the regime of targeted therapies, it is evident that this is likely to become a major problem in the future as more kinase inhibitors are used to treat larger patient populations. As gleaned from the emergence of resistance to antimicrobial or antiviral agents by way of chemical inactivation of essential proteins and selective pressures that increase the incidence of mutations that convey said resistance, cancer cells carrying these mutations will also become more pronounced in rapidly dividing cell populations. To account for this challenge and to stimulate the design of future generation kinase inhibitors, extensive investigations are underway to

Figure 3. 1,3-Substituted hybrid (**3e**) docked to drug resistant cSrc-T338M. The 1,3-meta hybrid compound **3e** (green) was docked manually into wild type cSrc-**3b** (a) and drug resistant cSrc-T338M-**3b** (b) complexes. Care was taken to conserve the essential hydrogen bonding interaction of the quinazoline N1 with the backbone of the hinge region and occupation of the allosteric site by the pyrazolourea moiety. The inhibitor adopts a binding mode well tolerated by a small gatekeeper residue (T338). (c) In drug resistant cSrc-T338M, the central 1,4-substituted phenyl element of **3a**−**c** can freely rotate to adapt to a larger gatekeeper residue. (d) Free rotation of this crucial element in 1,3-substituted hybrid compounds is not possible and would result in either loss of the backbone hydrogen bond or displacement of the pyrazolourea from the allosteric site to accommodate the larger gatekeeper. Decreased inhibitor flexibility helps to explain why binding of **3d** and **3e** to drug resistant cSrc-T338M is significantly compromised.

provoke drug resistance formation in model organisms treated with specific kinase inhibitors with the hope of uncovering future clinically relevant mutant kinase alleles to be used as predictive markers. Such knowledge will advance the concept of personalized cancer therapies by using the compounds best suited for the identified tumor cell type.[43−45] In an alternative approach, knowledge about which position(s) is likely to develop relevant drug resistance mutations in kinases will be crucial for the design of next generation drugs that can overcome them. Although kinases remain one of the largest classes of enzymes studied, strategies for overcoming drug resistance are a challenging task and innovative solutions still need to be found. For example, Crespo et al.[46] showed that imatinib can be re-engineered to minimize the entropic cost of binding to drug resistant D816V Abl mutant by promoting disorder in the DFG loop. Our results illustrate a powerful alternative rationale to overcome drug resistance by generating type II inhibitors that have the intrinsic ability to adapt to the binding site distortions induced by these mutations while also locking the kinase in an inactive conformation.

Experimental Section

Chemistry. Unless otherwise noted, all reagents and solvents were purchased from Acros, Fluka, Sigma, Aldrich, or Merck and used without further purification. Dry solvents were purchased as anhydrous reagents from commercial suppliers. ^{1}H and ^{13}C NMR spectra were recorded on a Bruker Avance DRX 400 spectrometer

at 400 and 101 MHz, respectively. ^{1}H chemical shifts are reported in δ (ppm) as s (singlet), d (doublet), dd (doublet of doublet), t (triplet), q (quartet), m (multiplet), and bs (broad singlet) and are referenced to the residual solvent signal: CDCl$_3$ (7.26), DMSO-d_6 (2.50). ^{13}C spectra are referenced to the residual solvent signal: CDCl$_3$ (77.0) or DMSO-d_6 (39.0). All final compounds were purified to >95% purity, as determined by high-performance liquid chromatography (HPLC) (Supporting Information Table 3). Purity was measured using Agilent 1200 series HPLC systems with UV detection at 210 nm (system: Agilent Eclipse XDB-C18 4.6 mm × 150 mm, 5 μM, 10−100% CH$_3$CN in H$_2$O, with 0.1% TFA, for 15 min at 1.0 mL/min). High resolution electrospray ionization mass spectra (ESI-FTMS) were recorded on a Thermo LTQ Orbitrap (high resolution mass spectrometer from Thermo Electron) coupled to an "Accela" HPLC system supplied with a "Hypersil GOLD" column (Thermo Electron). Analytical TLC was carried out on Merck 60 F245 aluminum-backed silica gel plates. Compounds were purified by column chromatography using Baker silica gel (40−70 μm particle size). Preparative HPLC was conducted on a Varian HPLC system (Pro Star 215) with a VP 250/21 nucleosil C18 PPN column from Macherey-Nagel and monitored by UV at $\lambda = 254$ nm.

3-*tert*-Butyl-1-*m*-tolyl-1*H*-pyrazol-5-amine (4a).[47] To a solution of *m*-tolylhydrazine (0.5 g, 3.96 mmol) and 4,4-dimethyl-3-oxopentanenitrile (0.49 g, 3.96 mmol) in EtOH (10 mL) was added concentrated HCl (2 mL), and the reaction mixture was refluxed at 90 °C for 24 h. The volatiles were removed in vacuo, and water was added and extracted with DCM (3 × 30 mL). The combined organic layers were washed with saturated NaHCO$_3$ (1 × 30 mL)
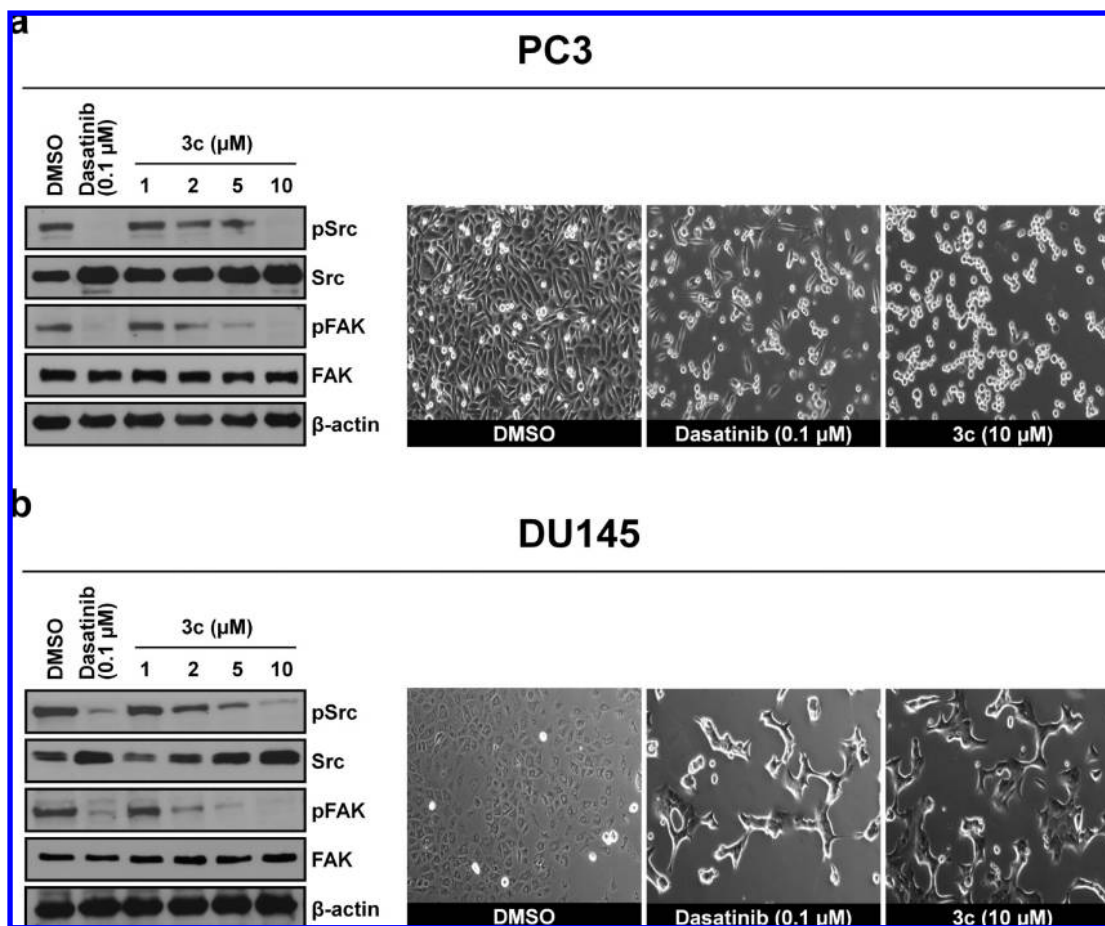
Figure 4. Reduction of cell-to-cell-contacts and cell proliferation in PC3 and DU145 cells by **3c**. PC3 (a) and DU145 (b) cells were treated for 5 h with **3c** (1, 2, 5, and 10 μM), dasatinib (100 nM), or vehicle (DMSO). Cells were lysed and blotted for indicated proteins. pSrc and pFAK levels are markedly reduced in response to treatment with **3c** and dasatinib (left panel). Total expression of FAK was unchanged, while cSrc expression was increased in both cell lines. Cell-to-cell contacts visualized by light microscopy at 10× magnification. PC3 and DU145 cells show markedly reduced cell-to-cell-contacts and fewer intact cells after treatment with **3c** (10 μM) or dasatinib (100 nM).

and dried over Na_2SO_4. Evaporation of the volatiles yielded the crude which was recrystallized from petrol ether/MeOH leading to 668 mg (74%) of colorless crystals: ^1H NMR (400 MHz, $CDCl_3$) δ 7.34 (s, 1H), 7.30 (d, $J = 4.7$ Hz, 2H), 7.10 (t, $J = 3.6$ Hz, 1H), 5.49 (s, 1H), 3.81 (s, 2H), 2.37 (s, 3H), 1.30 (s, 9H); ^{13}C NMR (101 MHz, $CDCl_3$) δ 162.23, 145.11, 139.80, 138.50, 129.34, 128.18, 125.20, 121.22, 87.67, 32.44, 30.51, 21.60. HRMS (ESI-MS) calcd: 230.165 17 for $C_{14}H_{20}N_3$ [M + H$^+$]. Found: 230.165 03.

2,2,2-Trichloroethyl 3-*tert*-Butyl-1-*m*-tolyl-1*H*-pyrazol-5-yl-carbamate (5).[48,49] A mixture of **4a** (500 mg, 2.2 mmol), H_2O (6 mL), EtOAc (10 mL), and NaOH (130 mg, 3.3 mmol) was stirred at 0 °C for 30 min. Then 2,2,2-trichloroethyl chloroformate (440 μL, 3.3 mmol) was added dropwise. After a further 30 min the ice bath was removed and the reaction mixture was stirred at room temperature for 2 h. The organic layer was separated from the aqueous layer which was extracted with EtOAc (4 × 10 mL). The combined organic layers were washed with brine twice, dried over Na_2SO_4, and evaporated in vacuo. The crude green solid was recrystallized from hexane to yield 536 mg (61%) of colorless crystals: ^1H NMR (400 MHz, $CDCl_3$) δ 7.35 (t, $J = 7.7$ Hz, 1H), 7.27 (s, 1H), 7.21 (t, $J = 7.6$ Hz, 2H), 6.87 (s, 1H), 6.40 (s, 1H), 4.79 (s, 2H), 2.39 (s, 3H), 1.33 (s, 9H); ^{13}C NMR (101 MHz, $CDCl_3$) δ 162.52, 150.98, 140.32, 137.78, 134.97, 129.70, 129.37, 126.09, 121.99, 95.04, 75.05, 32.65, 30.51, 21.59. HRMS (ESI-MS) calcd 404.063 93 for $C_{17}H_{21}O_2N_3^{35}Cl_3$ and 406.066 44 for $C_{17}H_{21}O_2N_3^{35}Cl_2^{37}Cl$ [M + H$^+$]. Found: 404.069 00 and 406.065 56.

General Procedure for the Preparation of Aminophenyl-3-(3-*tert*-butyl-1-tolyl-1*H*-pyrazol-5-yl)urea Hydrochlorides (7a,b).[48,49] *N*-Boc-phenylenediamine was dissolved in dry DMSO and treated with DIPEA. The reaction mixture was placed under argon and stirred at room temperature for 10 min before **4a** was added in one portion. The reaction mixture was heated to 60 °C for 3 h. After cooling to room temperature, the mixture was portioned between EtOAc and H_2O. The aqueous layer was extracted with EtOAc (3 × 10 mL). The combined organic layer was washed with brine and H_2O, dried over Na_2SO_4, and evaporated in vacuo. A solution of the obtained solid and HCl (4 M solution in dioxane) in dioxane was stirred at room temperature for 30 min before the volatiles were removed in vacuo. The product was used without further purification.

1-(4-Aminophenyl)-3-(3-*tert*-butyl-1-*m*-tolyl-1*H*-pyrazol-5-yl)urea Hydrochloride (7a). 7a was prepared as described above in the general procedure using *N*-Boc-*p*-phenylenediamine (157 mg, 0.8 mmol), DMSO (2 mL), DIPEA (400 μL, 2.3 mmol), **5** (305 mg, 0.8 mmol). The crude material was purified on silica gel (30−100% EtOAc/petrol ether) to yield 339 mg (96%) of the off-white solid product *tert*-butyl 4-(3-(3-*tert*-butyl-1-*m*-tolyl-1*H*-pyrazol-5-yl)ureido)phenylcarbamate (**6a**). Then **6a** (339 mg, 0.7 mmol), HCl (4 mL of a 4 M solution in dioxane), and dioxane (1 mL) were used. Without further purification, an amount of 249 mg (86%) of the off-white solid product **7a** was obtained: ^1H NMR (400 MHz, DMSO-d_6) δ 10.27 (bs, 2H), 9.78 (s, 1H), 8.83 (s, 1H), 7.51 (d, $J = 8.8$ Hz, 2H), 7.35 (m, 5H), 7.21 (d, $J = 7.3$ Hz, 1H), 6.37 (s, 1H), 2.37 (s, 3H), 1.28 (s, 9H); ^{13}C NMR (101 MHz, DMSO-d_6) δ 160.54, 151.83, 139.44, 138.87, 138.08, 137.18, 129.06, 128.08, 125.14, 124.94, 123.86, 121.41, 118.72, 95.96, 32.06, 30.18, 20.99. HRMS (ESI-MS) calcd: 364.213 19 for $C_{21}H_{26}N_5O$ [M + H$^+$]. Found: 364.213 15.

1-(3-Aminophenyl)-3-(3-*tert*-butyl-1-*m*-tolyl-1*H*-pyrazol-5-yl)urea Hydrochloride (7b). 7b was prepared as described above in the general procedure using *N*-Boc-*m*-phenylenediamine (92 mg, 0.4 mmol), DMSO (2 mL), DIPEA (150 μL, 0.9 mmol), **5** (180 mg, 0.6 mmol). The reaction mixture was heated to 60 °C for 24 h. The crude material was purified on silica gel (30−50% EtOAc/ petrol ether), yielding 150 mg (74%) of the off-white solid product *tert*-butyl 3-(3-(3-*tert*-butyl-1-*m*-tolyl-1*H*-pyrazol-5-yl)ureido)phe-nyl carbamate (**6b**). Then **6b** (150 mg, 0.3 mmol), HCl (3 mL of a 4 M solution in dioxane), and dioxane (1 mL) were used. Without further purification, an amount of 120 mg (92%) of the white product **7b** was obtained: ^{1}H NMR (400 MHz, DMSO-d_6) δ 9.98 (s, 1H), 8.91 (s, 1H), 7.65 (s, 1H), 7.40−7.32 (m, 5H), 7.21 (d, *J* = 7.35 Hz, 1H), 6.98 (m, 1H), 6.38 (s, 1H), 2.38 (s, 3H), 1.28 (s, 9H); ^{13}C NMR (101 MHz, DMSO-d_6) δ 160.55, 151.81, 140.76, 138.90, 138.06, 137.09, 132.08, 130.14, 129.08, 128.10, 124.91, 121.37, 117.26, 116.49, 112.44, 96.07, 32.07, 30.18, 21.01. HRMS (ESI-MS) calcd: 364.213 19 for $C_{21}H_{26}N_5O$ [M + H$^+$]. Found: 364.213 16.

6-Nitroquinazolin-4-ol (11). A solution of 2-amino-5-nitroben-zoic acid (9.5 g, 52 mmol) and formamidine acetate (22.0 g, 210 mmol) in 2-methoxyethanol (300 mL) was refluxed at 132 °C overnight and then concentrated in vacuo. The precipitate was filtered and washed with MeOH to yield 7.95 g (79%) of a brown powder. The product was used without further purification: ^{1}H NMR (400 MHz, DMSO-d_6) δ 12.70 (s, 1H), 8.71 (s, 1H), 8.48 (d, *J* = 7.5 Hz, 1H), 8.27 (s, 1H), 7.79 (d, *J* = 8.4 Hz, 1H); ^{13}C NMR (101 MHz, DMSO-d_6) δ 160.54, 152.89, 148.92, 144.88, 129.00, 128.18, 3c.64, 121.86. HRMS (ESI-MS) calcd: 192.040 37 for $C_8H_6N_3O_3$ [M + H$^+$]. Found: 192.040 18.

General Procedure for the Preparation of 1-(3-*tert*-Butyl-1-*m*-tolyl-1*H*-pyrazol-5-yl)-3-((6-nitroquinazolinylamino)phenyl)-ureas (3a,d). A two-neck flask was flushed with argon and charged with **11** and thionyl chloride. A catalytic amount of DMF was added, and the reaction mixture was refluxed at 78 °C overnight. The thionyl chloride was evaporated under reduced pressure. The residue was dissolved in DCM and filtered over silica gel to give 4-chloro-6-nitroquinazoline (**12**) which was dried under high vacuum and used without further purification. A solution of pyrazolourea hydrochloride **7a,b** and DIPEA in DCM was stirred for 10 min before **12** was added in one portion. The reaction mixture was stirred at room temperature for 24 h. Saturated NaHCO₃ was added, and the organic layer was separated from the aqueous layer which was then extracted with EtOAc (4 × 10 mL). The combined organic layers were dried over Na₂SO₄ and the volatiles were removed in vacuo, yielding an orange solid. Further purification and characterization of each derivative are described below.

1-(3-*tert*-Butyl-1-*m*-tolyl-1*H*-pyrazol-5-yl)-3-(4-(6-nitroquinazo-lin-4-ylamino)phenyl)urea (3a). 3a was prepared as described above in the general procedure using **7a** (100 mg, 0.3 mmol), DIPEA (171 μL, 1 mmol), DCM (2 mL), and **10** (52 mg, 0.3 mmol). The reaction mixture was stirred at room temperature for 24 h. The crude was purified on silica gel (1−4% MeOH/DCM) to give 98 mg (73%) of the orange solid product: ^{1}H NMR (400 MHz, DMSO-d_6) δ 10.40 (s, 1H), 9.65 (d, *J* = 2.4 Hz, 1H), 9.11 (s, 1H), 8.67 (s, 1H), 8.54 (dd, *J* = 2.4, 9.2 Hz, 1H), 8.41 (s, 1H), 7.91 (d, *J* = 9.1 Hz, 1H), 7.72 (d, *J* = 8.9 Hz, 2H), 7.46 (m, 2H), 7.42 (d, *J* = 7.7 Hz, 1H), 7.34 (m, 2H), 7.24 (d, *J* = 7.43 Hz, 1H), 6.39 (s, 1H), 2.40 (s, 3H), 1.29 (s, 9H); ^{13}C NMR (101 MHz, DMSO-d_6) δ 160.11, 158.70, 157.86, 153.13, 151.54, 144.43, 138.91,138.43, 137.26, 136.17, 132.59, 129.42, 129.11, 128.01, 126.57, 125.06, 123.69, 121.51, 120.85, 118.12, 114.39, 94.95, 32.05, 30.24, 20.99. HRMS (ESI-MS) calcd: 537.235 71 for $C_{29}H_{29}N_8O_3$ [M + H$^+$]. Found: 537.235 18.

1-(3-*tert*-Butyl-1-*m*-tolyl-1*H*-pyrazol-5-yl)-3-(3-(6-nitroquinazo-lin-4-ylamino)phenyl)urea (3d). 3d was prepared as described above in the general procedure using **7b** (120 mg, 0.3 mmol), DIPEA (154 μL, 0.9 mmol), DCM (2 mL), and **10** (63 mg, 0.3 mmol). The crude was purified on silica gel (1−4% MeOH/DCM) to give 78 mg (49%) of the orange solid product: ^{1}H NMR (400 MHz, DMSO-d_6) δ 10.44 (s, 1H), 9.68 (d, *J* = 2.1 Hz, 1H), 9.17

(s, 1H), 8.70 (s, 1H), 8.55 (dd, *J* = 2.2, 9.2 Hz, 1H), 8.43 (s, 1H), 8.01 (s,1H), 7.93 (d, *J* = 9.2 Hz, 1H), 7.47 (d, *J* = 7.9 Hz, 1H), 7.43 (t, *J* = 7.7 Hz, 1H), 7.32 (dd, *J* = 7.5, 15.7 Hz, 3H), 7.24 (t, *J* = 6.9 Hz, 2H), 6.40 (s, 1H), 2.40 (s, 3H), 1.28 (s, 9H); ^{13}C NMR (101 MHz, DMSO-d_6) δ 160.61, 158.86, 157.68, 153.11, 151.41, 144.52, 139.62, 138.94, 138.81, 138.39, 137.24, 129.49, 129.13, 128.82, 128.05, 126.64, 125.12, 121.56, 120.98, 116.81, 114.45, 114.38, 112.64, 94.73, 32.05, 30.24, 20.99. HRMS (ESI-MS) calcd: 537.235 71 for $C_{29}H_{29}N_8O_3$ [M + H$^+$]. Found: 537.235 13.

General Procedure for the Preparation of (6-Aminoquinazo-lin-4-ylamino)phenyl)-3-(3-*tert*-butyl-1-*m*-tolyl-1*H*-pyrazol-5-yl)ureas (3b,e). A solution of **3a,d**, ammonium formate, and Pd/C in absolute EtOH was refluxed at 90 °C for 3 h. The reaction mixture was filtered over Celite, and the volatiles were removed in vacuo to yield the crude material which was purified on silica gel (2−5% MeOH/DCM). The silica gel was neutralized using DCM/5% Et₃N. Further purification and characterization of each derivative is described below.

1-(4-(6-Aminoquinazolin-4-ylamino)phenyl)-3-(3-*tert*-butyl-1-*m*-tolyl-1*H*-pyrazol-5-yl)urea (3b). 3b was prepared as described above in the general procedure using **3a** (86 mg, 0.16 mmol), ammonium formate (71 mg, 1.1 mmol), EtOH, and Pd/C. The product was obtained as 80 mg (98%) of a yellow powder: ^{1}H NMR (400 MHz, DMSO-d_6) δ 9.25 (s, 1H), 9.02 (s, 1H), 8.38 (s, 1H), 8.27 (s, 1H), 7.72 (d, *J* = 9.0 Hz, 2H), 7.50 (d, *J* = 8.8 Hz, 1H), 7.43 (d, *J* = 7.7 Hz, 1H), 7.36 (m, 5H), 7.28 (d, *J* = 25.1 Hz, 1H), 7.22 (dd, *J* = 2.3, 8.9 Hz, 1H), 6.38 (s, 1H), 5.51 (s, 2H), 2.40 (s, 3H), 1.29 (s, 9H); ^{13}C NMR (101 MHz, DMSO-d_6) δ 160.64, 156.02, 151.57, 149.97, 147.13, 142.40, 138.89, 138.45, 137.36, 134.70, 134.34, 129.09, 128.57, 127.98, 125.05, 123.41, 3c.58, 121.50, 118.25, 116.57, 101.12, 94.88, 32.05, 30.24, 20.99. HRMS (ESI-MS) calcd: 507.261 53 for $C_{29}H_{31}N_8O$ [M + H$^+$]. Found: 507.260 84.

1-(3-(6-Aminoquinazolin-4-ylamino)phenyl)-3-(3-*tert*-butyl-1-*m*-tolyl-1*H*-pyrazol-5-yl)urea (3e). 3e was prepared as described above in the general procedure using **3d** (50 mg, 0.09 mmol), ammonium formate (41 mg, 0.7 mmol), EtOH (1.5 mL), and Pd/C. The crude material was purified on silica gel (2−5% MeOH/DCM). In a second purification step the product was purified by HPLC (MeCN/H₂O with 0.1% TFA) to yield 17 mg (36%) of the free base as a green powder: ^{1}H NMR (400 MHz, DMSO-d_6) δ 9.31 (s, 1H), 9.08 (s, 1H), 8.40 (s, 1H), 8.31 (s, 1H), 7.98 (s, 1H), 7.52 (d, *J* = 8.8 Hz, 1H), 7.38 (m, 5H), 7.23 (m, 4H), 6.40 (s, 1H), 5.57 (s, 2H), 2.39 (s, 3H), 1.28 (s, 9H); ^{13}C NMR (101 MHz, DMSO-d_6) δ 160.66, 156.00, 151.36, 149.76, 147.14, 142.55, 140.38, 139.39, 138.93, 138.38, 137.34, 129.12, 128.62, 128.05, 125.14, 123.58, 121.58, 116.75, 116.55, 115.66, 112.78, 111.46, 101.16, 94.54, 32.04, 30.24, 20.98. HRMS (ESI-MS) calcd: 507.261 53 for $C_{29}H_{31}N_8O$ [M + H$^+$]. Found: 507.260 83.

***N*-(4-(4-(3-(3-*tert*-Butyl-1-*m*-tolyl-1*H*-pyrazol-5-yl)ureido)phe-nylamino)quinazolin-6-yl)propionamide (3c).** A Schlenk tube was flushed with argon and charged with **3b** (15 mg, 29.61 μmol) and dry THF (1 mL), and the mixture was cooled to 0 °C before DIPEA (12.67 μL, 74.02 μmol) was added. A solution of propionyl chloride was prepared using 10 μL of propionyl chloride in 10 mL of dry THF. Then the solution of propionyl chloride (190 μL) was added dropwise to the reaction mixture which was stirred for 10 min before the ice bath was removed. After 1.5 h, an amount of 100 μL of the propionyl chloride solution was added and the mixture was stirred for a further 45 min until the reaction was complete. The mixture was basified with triethylamine before brine and EtOAc were added. The water phase was extracted with EtOAc (3 × 10 mL), and the combined organic layers were washed with water and dried over Na₂SO₄. The volatiles were removed in vacuo, leading to a yellow solid which was purified on silica gel using DCM/1−4% MeOH. An amount of 12 mg (72%) of the yellow solid product was obtained: ^{1}H NMR (400 MHz, DMSO-d_6) δ 10.31 (s, 1H), 9.73 (s, 1H), 9.39 (bs, 1H), 8.89 (bs, 1H), 8.70 (s, 1H), 8.44 (s, 1H), 7.86 (d, *J* = 9.0 Hz, 1H), 7.68 (dd, *J* = 8.9, 16.8 Hz, 3H), 7.40 (m, 5H), 7.20 (d, *J* = 6.6 Hz, 1H), 6.35 (s, 1H), 2.43 (m, 5H), 1.28 (s, 9H), 1.13 (t, *J* = 7.5 Hz, 3H); ^{13}C NMR (101 MHz, DMSO-d_6) δ

172.49, 160.92, 157.82, 153.61, 152.38, 146.63, 139.11, 138.92, 137.74, 137.18, 135.86, 133.95, 129.34, 128.46, 128.12, 127.19, 125.14, 123.58, 121.59, 118.40, 115.73, 112.26, 96.12, 32.40, 30.60, 29.71, 21.35, 10.01. HRMS (ESI-MS) calcd: 563.287 75 for $C_{32}H_{35}N_8O_2$ [M + H$^+$]. Found: 563.287 26.

Kinase Expression and Purification. N-Terminal His tag constructs of human p38α and chicken cSrc (residues 251−533) containing a PreScission protease cleavage site were expressed and purified from *E. coli*. The p38α construct was cloned into a pOPINE vector and was transformed as an N-terminal His-tag construct with Precision protease cleavage site into BL21(DE3) *E. coli*. Cultures were grown at 37 °C until an OD_{600} of 0.6 was attained, cooled in 30 min to room temperature, and then induced with 1 mM IPTG for overnight (∼20 h) expression at 18 °C while shaking at 160 rpm. Cells were lysed in buffer A (50 mM Tris, pH 8.0, 500 mM NaCl + 5% glycerol + 25 mM imidazole) and loaded onto a 30 mL Ni column (self-packed), washed with 3 column volumes (CV) of Ni buffer A and then eluted with a 0−50% linear gradient using Ni buffer B (Ni buffer A + 500 mM imidazole) over 2 CV. The protein was cleaved by incubating with PreScission protease (50 μg/mL final concentration) in a 12−30 mL capacity 10-MWCO dialysis cassette (Thermo Scientific) overnight at 4 °C in dialysis buffer (50 mM Tris, pH 7.5, 5% glycerol, 150 mM NaCl, 1 mM EDTA, 1 mM DTT). The protein was then centrifuged for 15 min at ∼13 000 rpm to remove any precipitate that may have formed during the cleavage step. The supernatant was then taken and diluted at least 4-fold in anion buffer A (50 mM Tris, pH 7.4, 5% glycerol, 50 mM NaCl, 1 mM DTT) and loaded onto a 1 mL Sepharose Q FF column (GE Healthcare) and washed with 10 CV of anion buffer A. The protein was eluted with a 0−100% linear gradient of anion buffer B (anion buffer A + 600 mM NaCl) over 20 CV. The protein was pooled and concentrated down to 2 mL and passed through a Sephadex HiLoad 26/60 Superdex 75 column equilibrated with size exclusion buffer (20 mM Tris, pH 7.4, 5% glycerol, 200 mM NaCl, 1 mM DTT) at a rate of 2 mL/min. The eluted protein was then concentrated to ∼10 mg/mL, aliquoted, and frozen at −80 °C. The chicken cSrc gene (residues 251−533) was codon-usage optimized for bacterial expression and synthesized synthetically (Geneart AG, Regensburg, Germany). The chicken cSrc gene was cloned into a pOPINF vector to generate an N-terminal His tag construct containing a PreScission protease cleavage site. The plasmid was transformed into BL21(DE3) codon + RIL *E. coli* for expression. Briefly, cultures shaking at 200 rpm were grown in TB media (containing 1% w/v glucose, chloramphenicol, and ampicillin) until an OD_{600} of ∼0.2 was attained. The cultures were then cooled to 20 °C for 1 h prior to induction with 0.3 mM IPTG. The expression continued overnight (approximately 20 h) at 20 °C. The protein was purified using protocols similar to those described previously,[14,50] with the exception of using PreScission protease (50 μg/mL final concentration) to cleave the N-terminal His tag. Following size exclusion, the eluted protein was concentrated to ∼10 mg/mL in size exclusion buffer (50 mM Tris, pH 8.0, 100 mM NaCl, 5% v/v glycerol, 1 mM DTT), aliquoted, and frozen at −80 °C.

Analysis of cSrc Labeling by HPLC and Mass Spectrometry. Proteins were trypsinized according to standard procedures prior to HPLC and mass spectrometry analysis to confirm the conjugation of the fluorophore to the desired protein fragment. Unlabeled and labeled cSrc (60 μg) samples were incubated separately with proteomics grade trypsin (3 μg) in 55 mM NH_4CO_3 with 10% v/v acetonitrile. Samples were incubated overnight at 37 °C, frozen in liquid nitrogen, and lyophilized. The lyophilized powder was then resuspended in 75 μL of water for analysis. Digested peptide fragments were then separated and purified using an HPLC (Agilent 1100 series) equipped with a binary pump, thermostated autosampler, and diode array detector. Samples were passed through a Waters (Milford, MA) Atlantis dC18 column (2.1 mm × 150 mm) with 3 μm particle size at ambient temperature. Samples were run at 0.2 mL/min with the following gradient: 100% solvent A (0.1% formic acid in water) for 5 min, ramping up to 60% solvent B (0.1% formic in acetonitrile) with a linear gradient in 55 min, then increasing to 80% solvent B in 10 min before holding at 80%

solvent B until 90 min. The mass spectrometer (Thermo LTQ) was equipped with a standard electrospray ion source (source voltage of 4 kV). An automatic MS/MS analysis was performed for the most intense peaks (minimal signal intensity of 10 000 required) in a triple play experiment (normal MS, zoom scan of the most intense peaks, followed by MS/MS in the case where the charge state was 2 or higher). A 35% normalized collision energy was used for MS/MS analysis.

Determination of K_d, k_{on}, k_{off}. Fluorophore labeled kinases were generated as previously described.[20] Screening initiatives were carried out for acrylodan-labeled cSrc in 384-well plates. Stocks of candidate compounds were prepared in DMSO at 20× the final desired concentration. Compounds were mixed with labeled cSrc in triplicate at final concentrations of 10 and 50 μM. Each well contained 1 μL of compound and 19 μL of measurement buffer (+0.01% v/v Brij-35) containing 100 nM kinase (5% v/v DMSO after mixing). Plates were covered with an adhesive aluminum foil and incubated for 15−30 min at room temperature prior to measurement of emission intensities at 445, 475, and 505 nm using a Tecan Safire^2 plate reader. Acrylodan was excited at 386 nm. Binding was measured using a ratio of $\lambda 445/\lambda 475$ while inhibitor binding mode (DFG-in or DFG-out) was revealed by the ratio of $\lambda 505/\lambda 475$. Potential hits were subjected to further titration studies in cuvettes or 96-well plates to obtain K_d values. Kinetic measurements were made by placing labeled cSrc into cuvettes with a rapidly stirring mini stir bar and monitoring changes in acrylodan fluorescence upon addition of a single dose of each inhibitor. Inhibitors were dissolved in 100% DMSO stocks and delivered to the sample through the injection port above the sample chamber. At equilibrium, a 10-fold excess of unlabeled kinase was added to extract the bound inhibitor from the labeled kinase. The resulting fluorescence changes from binding and dissociation of the ligand were well fitted to a first-order decay function to determine the observed rate constants for dissociation (k_{off}) as well as binding (k_{on}) for a single dose of each compound.

Crystallization and Structure Determination of cSrc-dasatinib, cSrc-3b and cSrc-T338M-3b. For the cSrc-**dasatinib**, cSrc-**3b** and cSrc-T338M-**3b** complex structures, 500 μM inhibitor (prepared in DMSO) was pre-incubated along with 180 μM wild type cSrc or cSrc-T338M (stored in 20 mM Tris pH 8.0, 100 mM NaCl, 1 mM DTT) for 4 hr to form the enzyme−inhibitor complex prior to crystallization. In the case of dasatinib, crystals were grown using the hanging drop method at (20 °C) after mixing 1 μL protein−inhibitor solution with 0.5 μL reservoir solution (122 mM MES (pH 6.4), 11% PEG 20000, 22.5% (v/v) glycerol). In the case of **3b**, crystals were grown using the sitting drop method at (20 °C) after mixing 0.2 μL protein−inhibitor complex and 0.2 μL reservoir solution (85 mM MES (pH 6.5), 10.2% PEG 20000, 15% (v/v) glycerol). Drops were pipetted using a Mosquito Nanodrop crystallization robot (TTP LabTech Ltd., Melbourn, UK). All crystals were directly frozen without the addition of glycerol. Diffraction data of all cSrc−inhibitor complex crystals were collected at the PX10SA beamline of the Swiss Light Source (PSI, Villingen, Switzerland) to a resolution of 2.2 Å for cSrc-dasatinib and 2.6 Å for cSrc-**3b** and cSrc-T338M-**3b**, using wavelengths close to 1 Å. All data sets were processed with XDS[51] and scaled using XSCALE.[51]

Structure Determination and Refinement of cSrc-Dasatinib, cSrc-3b, and cSrc-T338M-3b. All three cSrc−inhibitor complex structures were solved by molecular replacement with PHASER[52] using the published cSrc structure 2OIQ[53] as template. The two cSrc molecules in the asymmetric unit were manually modified using the program COOT.[54] The model was first refined with CNS[55] using simulated annealing to remove model bias. The final refinement was performed with REFMAC5.[56] Inhibitor topology files where generated using the Dundee PRODRG2 server.[57] Refined structures were validated with PROCHECK.[58] Detailed data, refinement, and Ramachandran statistics are in Supporting Information Table 1. PyMOL[59] was used to produce the figures.

Kinetics Assay for IC$_{50}$ Determination. IC$_{50}$ determinations for cSrc kinases were measured with the HTRF KinEASE™-TK assay from Cisbio according to the manufacturer's instructions. A biotinylated poly-Glu-Tyr substrate peptide was phosphorylated by cSrc. After completion of the reaction, an anti-phosphotyrosine antibody labeled with europium cryptate and streptavidin labeled with the fluorophore XL665 were added. The FRET between europium cryptate and XL665 was measured to quantify the phosphorylation of the substrate peptide. ATP concentrations were set at their respective K_m values (15 μM for the wild type cSrc and 1 μM for cSrc-T338M), and 100 nM substrate was used for both wild type and drug resistant cSrc. Kinase, substrate peptide, and inhibitor were preincubated for 2 h before the reaction was started by addition of ATP. A Tecan Safire^2 plate reader was used to measure the fluorescence of the samples at 620 nm (Eu-labeled antibody) and 665 nm (XL665 labeled streptavidin) 60 μs after excitation at 317 nm. The quotient of both intensities for reactions made with eight different inhibitor concentrations was fit to a Hill four-parameter equation to determine IC$_{50}$ values. Each reaction was performed in duplicate, and at least three independent determinations of each IC$_{50}$ were made.

Cell Culture. PC3 and DU145 were generously provided by Dr. Roman Thomas (Max Planck Institute for Neurological Research, Cologne, Germany). The cells were cultured in Dulbecco's modified Eagle's medium (DMEM) supplemented with 10% heat-inactivated fetal bovine serum (FBS) and 100 units/mL penicillin per streptomycin. Cells were cultured at 37 °C in humidified air containing 5% CO$_2$. After inhibitor treatment (5 h), the cells were washed twice in cold phosphate-buffered saline (PBS) and then lysed for 10 min on ice in lysis buffer (20 mM Tris-HCl, pH 7.5, 150 mM NaCl, 1% Triton, 1 mM Na$_2$EDTA, 1 mM EGTA, 2.5 mM sodium pyrophosphate, 1 mM β-glycerophosphate, 1 mM Na$_3$VO$_4$, 1 μg/mL leupeptin, 1 mM PMSF, and common protease inhibitors). Subsequently, cells were centrifuged for 20 min at 20000g and at 4 °C. The supernatant was subjected to immunoblot analysis.

Immunoblot Analysis of Src and FAK. Protein concentration was measured using a spectrophotometer (ND-1000, peQLab). Equal amounts of protein were separated by SDS−PAGE and transferred to nitrocellulose membranes. Blots were blocked for 1 h in Tris-buffered saline with Tween-20 (TBST) supplemented with 5% nonfat milk and subsequently incubated overnight at 4 °C in primary antibody, namely, anti-phospho-FAK, anti-phospho-Src, anti-FAK, and anti-Src. All antibodies were obtained from Cell Signaling Technology. After being washed, blots were incubated with secondary antibodies and then detected on film using the enhanced chemiluminescence (ECL) detection system.

Supporting Information Available: The crystal structure of dasatinib in complex with cSrc, synthesis scheme of pyrazoloureas, **1b** modeled into the binding site of drug resistant cSrc-T338M, 1,3-meta and 1,4-para hybrid compounds modeled to inactive human p38α, kinase selectivity profiles for **3b** and **3e**, rate constants for the dissociation of **3a−e** from acrylodan-labeled cSrc, table of compound purities, and crystal X-ray structure data for **3b** and dasatinib. This material is available free of charge via the Internet at http://pubs.acs.org.

References

(1) Gschwind, A.; Fischer, O. M.; Ullrich, A. The discovery of receptor tyrosine kinases: targets for cancer therapy. *Nat. Rev. Cancer* **2004**, *4*, 361–370.

(2) Backes, A. C.; Zech, B.; Felber, B.; Klebl, B.; Müller, G. Small-molecule inhibitors binding to protein kinases. Part I: exceptions from the traditional pharmacophore approach of type I inhibition. *Expert Opin. Drug Discovery* **2008**, *3*, 1409–1425.

(3) Backes, A. C.; Zech, B.; Felber, B.; Klebl, B.; Müller, G. Small-molecule inhibitors binding to protein kinase. Part II: the novel pharmacophore approach of type II and type III inhibition. *Expert Opin. Drug Discovery* **2008**, *3*, 1427–1449.

(4) Zhang, J.; Yang, P. L.; Gray, N. S. Targeting cancer with small molecule kinase inhibitors. *Nat. Rev. Cancer* **2009**, *9*, 28–39.

(5) Bikker, J. A.; Brooijmans, N.; Wissner, A.; Mansour, T. S. Kinase domain mutations in cancer: implications for small molecule drug design. *J. Med. Chem.* **2009**, *52*, 1493–1509.

(6) Liu, Y.; Gray, N. S. Rational design of inhibitors that bind to inactive kinase conformations. *Nat. Chem. Biol.* **2006**, *2*, 358–364.

(7) Apsel, B.; Blair, J. A.; Gonzalez, B.; Nazif, T. M.; Feldman, M. E.; Aizenstein, B.; Hoffman, R.; Williams, R. L.; Shokat, K. M.; Knight, Z. A. Targeted polypharmacology: discovery of dual inhibitors of tyrosine and phosphoinositide kinases. *Nat. Chem. Biol.* **2008**, *4*, 691–699.

(8) Du, J.; Bernasconi, P.; Clauser, K. R.; Mani, D. R.; Finn, S. P.; Beroukhim, R.; Burns, M.; Julian, B.; Peng, X. P.; Hieronymus, H.; Maglathlin, R. L.; Lewis, T. A.; Liau, L. M.; Nghiemphu, P.; Mellinghoff, I. K.; Louis, D. N.; Loda, M.; Carr, S. A.; Kung, A. L.; Golub, T. R. Bead-based profiling of tyrosine kinase phosphorylation identifies SRC as a potential target for glioblastoma therapy. *Nat. Biotechnol.* **2009**, *27*, 77–83.

(9) Schenone, S.; Zanoli, S.; Brullo, C.; Crespan, E.; Maga, G. Current advances in the development of anticancer drugs targeting tyrosine kinases of the Src family. *Curr. Drug Ther.* **2008**, *3*, 158–176.

(10) Chang, Y. M.; Bai, L.; Liu, S.; Yang, J. C.; Kung, H. J.; Evans, C. P. Src family kinase oncogenic potential and pathways in prostate cancer as revealed by AZD0530. *Oncogene* **2008**, *27*, 6365–6375.

(11) Yeatman, T. J. A renaissance for SRC. *Nat Rev Cancer.* **2004**, *4*, 470–480.

(12) Daub, H.; Specht, K.; Ullrich, A. Strategies to overcome resistance to targeted protein kinase inhibitors. *Nat. Rev. Drug Discovery* **2004**, *3*, 1001–1010.

(13) Blencke, S.; Ullrich, A.; Daub, H. Mutation of threonine 766 in the epidermal growth factor receptor reveals a hotspot for resistance formation against selective tyrosine kinase inhibitors. *J. Biol. Chem.* **2003**, *278*, 15435–15440.

(14) Michalczyk, A.; Klüter, S.; Rode, H. B.; Simard, J. R.; Grütter, C.; Rabiller, M.; Rauh, D. Structural insights into how irreversible inhibitors can overcome drug resistance in EGFR. *Bioorg. Med. Chem.* **2008**, *16*, 3482–3488.

(15) Carter, T. A.; Wodicka, L. M.; Shah, N. P.; Velasco, A. M.; Fabian, M. A.; Treiber, D. K.; Milanov, Z. V.; Atteridge, C. E.; Biggs, W. H., 3rd; Edeen, P. T.; Floyd, M.; Ford, J. M.; Grotzfeld, R. M.; Herrgard, S.; Insko, D. E.; Mehta, S. A.; Patel, H. K.; Pao, W.; Sawyers, C. L.; Varmus, H.; Zarrinkar, P. P.; Lockhart, D. J. Inhibition of drug-resistant mutants of ABL, KIT, and EGF receptor kinases. *Proc. Natl. Acad. Sci. U.S.A.* **2005**, *102*, 11011–11016.

(16) Azam, M.; Seeliger, M. A.; Gray, N. S.; Kuriyan, J.; Daley, G. Q. Activation of tyrosine kinases by mutation of the gatekeeper threonine. *Nat. Struct. Mol. Biol.* **2008**, *15*, 1109–1118.

(17) Yun, C. H.; Mengwasser, K. E.; Toms, A. V.; Woo, M. S.; Greulich, H.; Wong, K. K.; Meyerson, M.; Eck, M. J. The T790M mutation in EGFR kinase causes drug resistance by increasing the affinity for ATP. *Proc. Natl. Acad. Sci. U.S.A.* **2008**, *105*, 2070–2075.

(18) Karaman, M. W.; Herrgard, S.; Treiber, D. K.; Gallant, P.; Atteridge, C. E.; Campbell, B. T.; Chan, K. W.; Ciceri, P.; Davis, M. I.; Edeen, P. T.; Faraoni, R.; Floyd, M.; Hunt, J. P.; Lockhart, D. J.; Milanov, Z. V.; Morrison, M. J.; Pallares, G.; Patel, H. K.; Pritchard, S.; Wodicka, L. M.; Zarrinkar, P. P. A quantitative analysis of kinase inhibitor selectivity. *Nat. Biotechnol.* **2008**, *26*, 127–132.

(19) Young, M. A.; Shah, N. P.; Chao, L. H.; Seeliger, M.; Milanov, Z. V.; Biggs, W. H., 3rd; Treiber, D. K.; Patel, H. K.; Zarrinkar, P. P.; Lockhart, D. J.; Sawyers, C. L.; Kuriyan, J. Structure of the kinase domain of an imatinib-resistant Abl mutant in complex with the Aurora kinase inhibitor VX-680. *Cancer Res.* **2006**, *66*, 1007–1014.

(20) (a) Simard, J. R.; Klüter, S.; Grütter, C.; Getlik, M.; Rabiller, M.; Rode, H. B.; Rauh, D. A new screening assay for allosteric inhibitors of cSrc. *Nat. Chem. Biol.*, doi: 10.1038/nchembio.162. (b) Simard,

J. R.; Getlik, M.; Grütter, C.; Pawar, V.; Wulfert, S.; Rabiller, M.; Rauh, D.; Development of a fluorescent-tagged kinase assay system for the detection and characterization of allosteric kinase inhibitors. *JACS* **2009**, in press.

(21) Dumas, J.; Hatoum-Mokdad, H.; Sibley, R.; Riedl, B.; Scott, W. J.; Monahan, M. K.; Lowinger, T. B.; Brennan, C.; Natero, R.; Turner, T.; Johnson, J. S.; Schoenleber, R.; Bhargava, A.; Wilhelm, S. M.; Housley, T. J.; Ranges, G. E.; Shrikhande, A. 1-Phenyl-5-pyrazolyl ureas: potent and selective p38 kinase inhibitors. *Bioorg. Med. Chem. Lett.* **2000**, *10*, 2051–2054.

(22) Pargellis, C.; Tong, L.; Churchill, L.; Cirillo, P. F.; Gilmore, T.; Graham, A. G.; Grob, P. M.; Hickey, E. R.; Moss, N.; Pav, S.; Regan, J. Inhibition of p38 MAP kinase by utilizing a novel allosteric binding site. *Nat. Struct. Biol.* **2002**, *9*, 268–272.

(23) Sharma, S. V.; Bell, D. W.; Settleman, J.; Haber, D. A. Epidermal growth factor receptor mutations in lung cancer. *Nat. Rev. Cancer* **2007**, *7*, 169–181.

(24) Hoelzemann, G.; Crassier, H.; Rautenberg, W. Pyrazole Derivatives Having Tyrosinkinase Activity. WO2007017083 (A1), 2007.

(25) Shuker, S. B.; Hajduk, P. J.; Meadows, R. P.; Fesik, S. W. Discovering high-affinity ligands for proteins: SAR by NMR. *Science* **1996**, *274*, 1531–1534.

(26) Nienaber, V. L.; Richardson, P. L.; Klighofer, V.; Bouska, J. J.; Giranda, V. L.; Greer, J. Discovering novel ligands for macromolecules using X-ray crystallographic screening. *Nat. Biotechnol.* **2000**, *18*, 1105–1108.

(27) Gill, A. L.; Frederickson, M.; Cleasby, A.; Woodhead, S. J.; Carr, M. G.; Woodhead, A. J.; Walker, M. T.; Congreve, M. S.; Devine, L. A.; Tisi, D.; O'Reilly, M.; Seavers, L. C.; Davis, D. J.; Curry, J.; Anthony, R.; Padova, A.; Murray, C. W.; Carr, R. A.; Jhoti, H. Identification of novel p38alpha MAP kinase inhibitors using fragment-based lead generation. *J. Med. Chem.* **2005**, *48*, 414–426.

(28) Jacobs, M. D.; Caron, P. R.; Hare, B. J. Classifying protein kinase structures guides use of ligand-selectivity profiles to predict inactive conformations: structure of lck/imatinib complex. *Proteins* **2008**, *70*, 1451–1460.

(29) Okram, B.; Nagle, A.; Adrian, F. J.; Lee, C.; Ren, P.; Wang, X.; Sim, T.; Xie, Y.; Xia, G.; Spraggon, G.; Warmuth, M.; Liu, Y.; Gray, N. S. A general strategy for creating "inactive-conformation" abl inhibitors. *Chem. Biol.* **2006**, *13*, 779–786.

(30) Warner, S. L.; Bashyam, S.; Vankayalapati, H.; Bearss, D. J.; Han, H.; Mahadevan, D.; Von, H. D. D.; Hurley, L. H. Identification of a lead small-molecule inhibitor of the Aurora kinases using a structure-assisted, fragment-based approach. *Mol. Cancer Ther.* **2006**, *5*, 1764–1773.

(31) Shewchuk, L.; Hassell, A.; Wisely, B.; Rocque, W.; Holmes, W.; Veal, J.; Kuyper, L. F. Binding mode of the 4-anilinoquinazoline class of protein kinase inhibitor: X-ray crystallographic studies of 4-anilino-quinazolines bound to cyclin-dependent kinase 2 and p38 kinase. *J. Med. Chem.* **2000**, *43*, 133–138.

(32) Heron, N. M.; Anderson, M.; Blowers, D. P.; Breed, J.; Eden, J. M.; Green, S.; Hill, G. B.; Johnson, T.; Jung, F. H.; McMiken, H. H.; Mortlock, A. A.; Pannifer, A. D.; Pauptit, R. A.; Pink, J.; Roberts, N. J.; Rowsell, S. SAR and inhibitor complex structure determination of a novel class of potent and specific Aurora kinase inhibitors. *Bioorg. Med. Chem. Lett.* **2006**, *16*, 1320–1323.

(33) Blair, J. A.; Rauh, D.; Kung, C.; Yun, C. H.; Fan, Q. W.; Rode, H.; Zhang, C.; Eck, M. J.; Weiss, W. A.; Shokat, K. M. Structure-guided development of affinity probes for tyrosine kinases using chemical genetics. *Nat. Chem. Biol.* **2007**, *3*, 229–238.

(34) Stamos, J.; Sliwkowski, M. X.; Eigenbrot, C. Structure of the epidermal growth factor receptor kinase domain alone and in complex with a 4-anilinoquinazoline inhibitor. *J. Biol. Chem.* **2002**, *277*, 46265–46272.

(35) Hunter, C. A.; Singh, J.; Thornton, J. M. Pi−pi interactions: the geometry and energetics of phenylalanine−phenylalanine interactions in proteins. *J. Mol. Biol.* **1991**, *218*, 837–846.

(36) Schaller, M. D. Biochemical signals and biological responses elicited by the focal adhesion kinase. *Biochim. Biophys. Acta* **2001**, *1540*, 1–21.

(37) Calalb, M. B.; Polte, T. R.; Hanks, S. K. Tyrosine phosphorylation of focal adhesion kinase at sites in the catalytic domain regulates kinase activity: a role for Src family kinases. *Mol. Cell. Biol.* **1995**, *15*, 954–963.

(38) Nowakowski, J.; Cronin, C. N.; McRee, D. E.; Knuth, M. W.; Nelson, C. G.; Pavletich, N. P.; Rogers, J.; Sang, B. C.; Scheibe, D. N.; Swanson, R. V.; Thompson, D. A. Structures of the cancer-related Aurora-A, FAK, and EphA2 protein kinases from nanovolume crystallography. *Structure* **2002**, *10*, 1659–1667.

(39) Owens, L. V.; Xu, L.; Craven, R. J.; Dent, G. A.; Weiner, T. M.; Kornberg, L.; Liu, E. T.; Cance, W. G. Overexpression of the focal adhesion kinase (p125FAK) in invasive human tumors. *Cancer Res.* **1995**, *55*, 2752–2755.

(40) Shor, A. C.; Keschman, E. A.; Lee, F. Y.; Muro-Cacho, C.; Letson, G. D.; Trent, J. C.; Pledger, W. J.; Jove, R. Dasatinib inhibits migration and invasion in diverse human sarcoma cell lines and induces apoptosis in bone sarcoma cells dependent on SRC kinase for survival. *Cancer Res.* **2007**, *67*, 2800–2808.

(41) Dar, A. C.; Lopez, M. S.; Shokat, K. M. Small molecule recognition of c-Src via the imatinib-binding conformation. *Chem. Biol.* **2008**, *15*, 1015–1022.

(42) Copeland, R. A.; Pompliano, D. L.; Meek, T. D. Drug−target residence time and its implications for lead optimization. *Nat. Rev. Drug Discovery* **2006**, *5*, 730–739.

(43) Bradeen, H. A.; Eide, C. A.; O'Hare, T.; Johnson, K. J.; Willis, S. G.; Lee, F. Y.; Druker, B. J.; Deininger, M. W. Comparison of imatinib mesylate, dasatinib (BMS-354825), and nilotinib (AMN107) in an *N*-ethyl-*N*-nitrosourea (ENU)-based mutagenesis screen: high efficacy of drug combinations. *Blood* **2006**, *108*, 2332–2338.

(44) von Bubnoff, N.; Veach, D. R.; van der Kuip, H.; Aulitzky, W. E.; Sanger, J.; Seipel, P.; Bornmann, W. G.; Peschel, C.; Clarkson, B.; Duyster, J. A cell-based screen for resistance of Bcr-Abl-positive leukemia identifies the mutation pattern for PD166326, an alternative Abl kinase inhibitor. *Blood* **2005**, *105*, 1652–1659.

(45) Zunder, E. R.; Knight, Z. A.; Houseman, B. T.; Apsel, B.; Shokat, K. M. Discovery of drug-resistant and drug-sensitizing mutations in the oncogenic PI3K isoform p110 alpha. *Cancer Cell* **2008**, *14*, 180–192.

(46) Crespo, A.; Zhang, X.; Fernandez, A. Redesigning kinase inhibitors to enhance specificity. *J. Med. Chem.* **2008**, *51*, 4890–4898.

(47) Regan, J.; Breitfelder, S.; Cirillo, P.; Gilmore, T.; Graham, A. G.; Hickey, E.; Klaus, B.; Madwed, J.; Moriak, M.; Moss, N.; Pargellis, C.; Pav, S.; Proto, A.; Swinamer, A.; Tong, L.; Torcellini, C. Pyrazole urea-based inhibitors of p38 MAP kinase: from lead compound to clinical candidate. *J. Med. Chem.* **2002**, *45*, 2994–3008.

(48) Bagley, M. C.; Davis, T.; Dix, M. C.; Widdowson, C. S.; Kipling, D. Microwave-assisted synthesis of *N*-pyrazole ureas and the p38alpha inhibitor BIRB 796 for study into accelerated cell ageing. *Org. Biomol. Chem.* **2006**, *4*, 4158–4164.

(49) Zhang, L. H.; Zhu, L. Novel Process for Synthesis of Heteroaryl-Substituted Urea Compounds. WO/2001/004115, 2001.

(50) Seeliger, M. A.; Young, M.; Henderson, M. N.; Pellicena, P.; King, D. S.; Falick, A. M.; Kuriyan, J. High yield bacterial expression of active c-Abl and c-Src tyrosine kinases. *Protein Sci.* **2005**, *14*, 3135–3139.

(51) Kabsch, W. Automatic processing of rotation diffraction data from crystals of initially unknown symmetry and cell constants. *J. Appl. Crystallogr.* **1993**, *26*, 795–800.

(52) Read, R. J. Pushing the boundaries of molecular replacement with maximum likelihood. *Acta Crystallogr., Sect. D: Biol. Crystallogr.* **2001**, *57*, 1373–1382.

(53) Seeliger, M. A.; Nagar, B.; Frank, F.; Cao, X.; Henderson, M. N.; Kuriyan, J. c-Src binds to the cancer drug imatinib with an inactive Abl/c-Kit conformation and a distributed thermodynamic penalty. *Structure* **2007**, *15*, 299–311.

(54) Emsley, P.; Cowtan, K. Coot: model-building tools for molecular graphics. *Acta Crystallogr., Sect. D: Biol. Crystallogr.* **2004**, *60*, 2126–2132.

(55) Brünger, A. T.; Adams, P. D.; Clore, G. M.; DeLano, W. L.; Gros, P.; Grosse-Kunstleve, R. W.; Jiang, J. S.; Kuszewski, J.; Nilges, M.; Pannu, N. S.; Read, R. J.; Rice, L. M.; Simonson, T.; Warren, G. L. Crystallography & NMR system: a new software suite for macromolecular structure determination. *Acta Crystallogr., Sect. D: Biol. Crystallogr.* **1998**, *54*, 905–921.

(56) Murshudov, G. N.; Vagin, A. A.; Dodson, E. J. Refinement of macromolecular structures by the maximum-likelihood method. *Acta Crystallogr., Sect. D: Biol. Crystallogr.* **1997**, *53*, 240–255.

(57) Schüttelkopf, A. W.; van Aalten, D. M. PRODRG: a tool for high-throughput crystallography of protein−ligand complexes. *Acta Crystallogr., Sect. D: Biol. Crystallogr.* **2004**, *60*, 1355–1363.

(58) Laskowski, R. A.; MacArthur, M. W.; Moss, D. S.; Thornton, J. M. PROCHECK: a program to check the stereochemical quality of protein structures. *J. Appl. Crystallogr.* **1993**, *26*, 283–291.

(59) DeLano, W. L. *The PyMOL Molecular Graphics System*; DeLano Scientific LLC: Palo Alto, CA, 2002; http://www.pymol.org.